SMAR 2019 – Fifth Conference on Smart Monitoring,
Assessment and Rehabilitation of Civil Structures

SMAR 2019

Local and Distortional Buckling Behaviour of Cold-Formed Steel Sigma Beam-Column Profiles

Ferhan ÖZTÜRK [1], Mehmet ŞENTÜRK [1,2], Selim PUL [1], Iman HAJIRASOULIHA [2]

[1] Karadeniz Technical University, Trabzon, Turkey

[2] The University of Sheffield, Sheffield, United Kingdom

Contact e-mail: senturkmeh@gmail.com

ABSTRACT: Cold-formed steel (CFS) sigma profiles generally used as purlins or portal frame members are shown in the literature to exhibit higher load carrying capacities compared to standard channel section profiles. However, currently CFS channel sections are more widely used, especially in residential buildings, due to ease of installation and also the knowledge about their structural performance gained through numerous experimental and numerical studies over last decades. To bridge the knowledge gap in using CFS sigma beam-column sections in common practice, this study aims to investigate the characteristic behaviour of these elements including their stiffness and strength under axial load and biaxial bending. In general, to determine the capacity of beam-column members, most existing design guidelines (e.g. AISI S213-07, AISI S100-12, AS/NZS 2005) suggest closed formed interaction formulas as a linear combination of axial load, and strong- and weak-axis bending moment effects. However, this approach ignores the nonlinear interactions between these actions. To address this issue, in this study, the structural behaviour of eccentrically loaded beam-column elements with CFS sigma profiles is investigated under simultaneous effects of axial loads and strong-and weak-axis bending (P-M_x-M_y). To this end, CUFSM software is used to determine the dominant buckling mode (i.e. local, distortional or global) and load carrying capacity of CFS sigma beam-column elements with different lengths. Material parameters are also implemented in the detailed finite element models developed in ABAQUS software. The models are then used to estimate the strength and buckling behaviour under monotonic loadings. A total of 315 finite element analyses are performed on different CFS beam-column elements with sigma profile and the results are compared with existing codes.

1 INTRODUCTION

Cold-formed steel members are widely used in many types of metal structures due to their advantages such as light-weight, high strength, fast and ease of installation. The cold-formed steel members which are subjected to combined axially compressing and bending loads should be designed as beam-column elements. Beam-columns generally require greater attention and calculation in analysis and design due to the interaction of the applied axial load and the bending moments. Current cold-formed steel design codes such as the North American Specification of the American Iron and Steel Institute (AISI S100-12), and the Australian/New Zealand Standard (AZ/NZS) for cold-formed steel structures (AS/NZS 2005) have adopted a linear interaction equation for combining the axial load and bending moments applied to beam-columns. Even though extensive efforts have been made to estimate the capacity of CFS members under pure axial or flexural actions (Hancock, 2003, Macdonald et al., 2008, Rondal, 2000, Young, 2008, Schafer, 2008) the design of structural members under explicit combined actions has been less investigated. As one of the few studies in this area, Torabian et al. (2015 and 2016) developed a

new DSM calculation method for beam-column members and Parastesh et al. (2019) on CFS beam-column shape optimization. To extend the knowledge of beam-column members, this paper numerically investigates the structural strength and stability of CFS Sigma section beam-columns under bi-axial moments and axial load and makes a comparison between FEA results and AISI strength calculations.

2 FINITE ELEMENT MODELING

In this study, the shell element, S9R5, in ABAQUS is used to model the CFS sigma sections. S9R5 is a quadratic thin shell element using Kirchhoff's constraint. Each node of this element has five degree of freedoms (three displacement components and two in-surface rotation components). S9R5 element has been shown to provide accurate predictions for thin-walled structures, and computationally is more efficient than other shell element alternatives such as S4, S4R and S8R5. In the thickness direction, seven integration points are used and cold roll-forming effect is ignored. The cross-section model is first built in CUFSM (Schafer and Adany, 2006) and eigenvalue buckling analysis is conducted to determine the expected imperfection modes. The CUFSM model is then exported to ABAQUS (via an input file) to run eigenvalue buckling analysis and use the same imperfection modes. A reference node is created at the mass centre of the cross-section at each end. The coordinate of the reference point varies as different eccentricities applied to the specimens. The nodal degrees of freedoms at the end of the specimen are coupled to the reference point using a beam type MPC constraint which forms a rigid link between the reference point and the end of the specimen with a length of 150 mm in the longitudinal direction. At the supporting end, all the translational degrees of freedom and the torsional degree of freedom of the reference point are constrained. At the loading end, the reference point is constrained in a similar way, except that the translational freedom in the longitudinal direction is released. Concentrated force is applied at the reference point in the longitudinal direction.

2.1 Material Model

To provide input data for FE models in ABAQUS, the engineering stress-strain curves obtained from tensile tests are converted to plastic true stress-true strain curves. The equation in Figure 1 is used to transfer the engineering stress-strain into true stress-strain. For the elastic part, the elastic Young's modulus is 200 GPa, the yield stress is 400 MPa, and the Poisson's ratio is 0.3. For the plastic part, von Mises yield rule, associated with flow and isotropic hardening is employed.

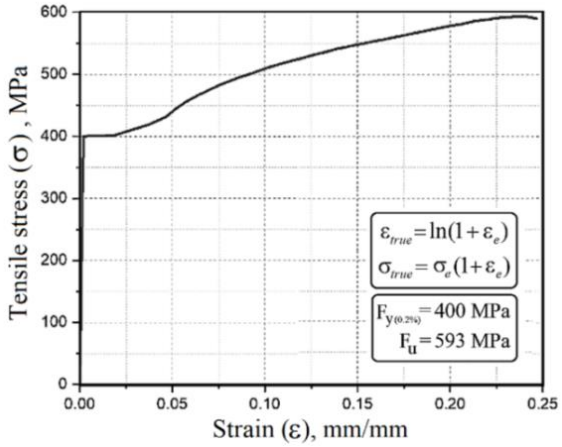

Figure 1. True stress-strain relation of the material.

In geometric and material nonlinear shell finite element collapse analyses, geometric imperfections are key to producing realistic strength predictions (Foroughi et al., 2014, Amouzegar et al., 2015 and Ye et al., 2018). Signs, combinations, and magnitudes of the geometric imperfection patterns are all important and finding the best ensemble requires measurements and sensitivity analyses. For local and distortional buckling modes, the sign of the imperfection may imply inward or outward flange or web deformations. Also, different signs of global imperfections can impose different local demands of the cross-section elements. Positive local and positive distortional buckling imperfection patterns generally provides lower-bound prediction of capacity. Therefore, in this study positive imperfection shapes are selected and imperfection magnitudes corresponding to the 50% CDF are utilised (see Table 1).

Table 1. Imperfection magnitudes δ or degrees from Zeinoddini and Schafer (2012)

CDF	Local (δ/t)	Distortional (δ/t)	Bowl (L/δ)	Camber (L/δ)	Twist (Deg/m)
25%	0.17	0.43	4755	6295	0.20
50%	0.31	0.75	2909	4010	0.30
75%	0.54	1.14	1659	2887	0.49

2.2 Specimen and Loading

Three different specimens for local, distortional and global buckling behaviour are investigated with length of 500 mm, 1000 mm, 1500 mm, respectively. The way used to apply axial load and boundary conditions are seen in Figure 2a and eccentricities are given in Table 2 in detail. A radial pattern is used for eccentric loading with an increment of 15° and 8 loading points used on each path as seen in Figure 2b.

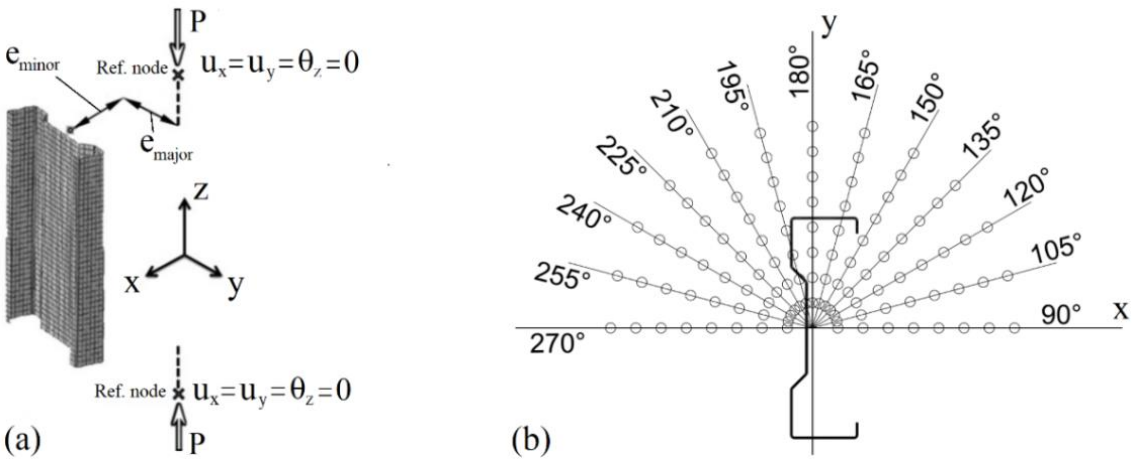

Figure 2. Eccentric loading and boundary conditions of FE model (a), loading pattern (b)

Nominal geometric properties of the specimens given by the producer of the cold-formed steel members used in this study are given in Figure 3. It should be noted that mid-thickness dimensions are needed for modelling the shell elements.

Table 2. Eccentricity values to apply axial load and bending moment.

Angle	Direction of Eccentricity	Eccentricities (mm) e1	e2	e3	e4	e5	e6	e7	e8
90º	e_x	25	50	75	100	125	150	175	200
	e_y	0	0	0	0	0	0	0	0
105º	e_x	24.15	48.30	72.44	96.59	120.74	144.89	169.04	193.19
	e_y	6.47	12.94	19.41	25.88	32.35	38.82	45.29	51.76
120º	e_x	21.65	43.30	64.95	86.60	108.25	129.90	151.55	173.21
	e_y	12.50	25.00	37.50	50.00	62.50	75.00	87.50	100.00
135º	e_x	17.68	35.36	53.03	70.71	88.39	106.07	123.74	141.42
	e_y	17.68	35.36	53.03	70.71	88.39	106.07	123.74	141.42
150º	e_x	12.50	25.00	37.50	50.00	62.50	75.00	87.50	100.00
	e_y	21.65	43.30	64.95	86.60	108.25	129.90	151.55	173.21
165º	e_x	6.47	12.94	19.41	25.88	32.35	38.82	45.29	51.76
	e_y	24.15	48.30	72.44	96.59	120.74	144.89	169.04	193.19
180º	e_x	0	0	0	0	0	0	0	0
	e_y	25	50	75	100	125	150	175	200
210º	e_x	21.65	43.30	64.95	86.60	108.25	129.90	151.55	173.21
	e_y	-12.50	-25.00	-37.50	-50.00	-62.50	-75.00	-87.50	-100.00
225º	e_x	17.68	35.36	53.03	70.71	88.39	106.07	123.74	141.42
	e_y	-17.68	-35.36	-53.03	-70.71	-88.39	-106.07	-123.74	-141.42
240º	e_x	12.50	25.00	37.50	50.00	62.50	75.00	87.50	100.00
	e_y	-21.65	-43.30	-64.95	-86.60	-108.25	-129.90	-151.55	-173.21
255º	e_x	6.47	12.94	19.41	25.88	32.35	38.82	45.29	51.76
	e_y	-24.15	-48.30	-72.44	-96.59	-120.74	-144.89	-169.04	-193.19
270º	e_x	0	0	0	0	0	0	0	0
	e_y	-25	-50	-75	-100	-125	-150	-175	-200

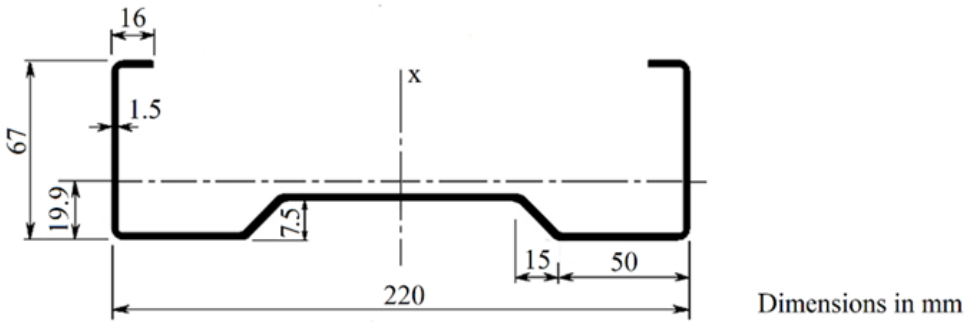

Figure 3. Cross-section properties of analysed specimens.

3 RESULTS

Shell finite element-based nonlinear material and geometric (GMNIA) collapse analyses are conducted in ABAQUS. Deformation shapes of beam-column members with length of 500 mm, 1000 mm and 1500 mm for axially loading, minor- and major axis bending are given in Figure 4. Also, cross-section deformation for the member with the length of 500 mm is given in Figure 5 for each loading angle. Axial load-deformation curves for eccentricities in e1 column in Table 2 are given in Figure 6 for each specimen lengths of 500 mm, 1000 mm and 1500 mm respectively.

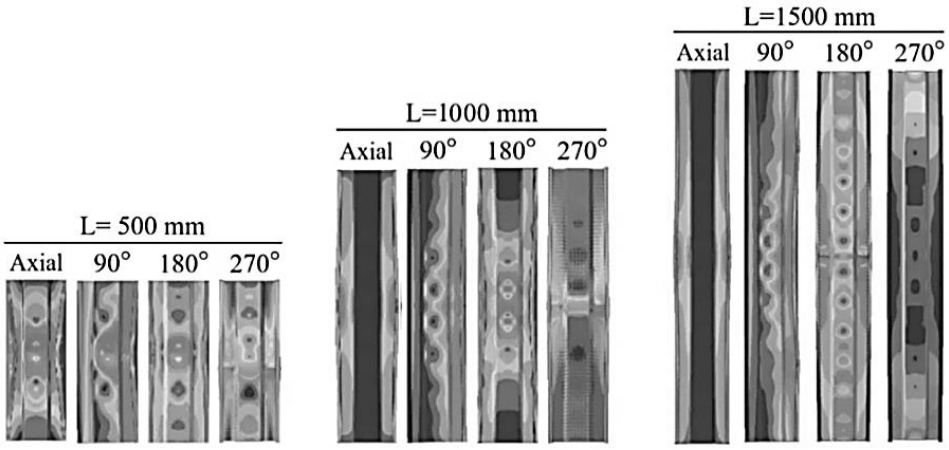

Figure 4. Deformation shapes of sigma profiles.

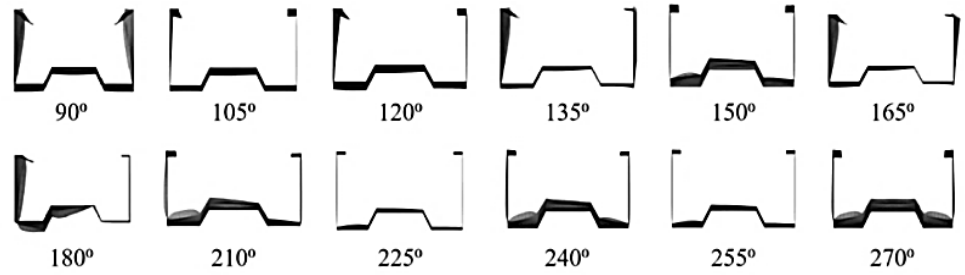

Figure 5. Deformation shapes of L=500 mm sigma profile.

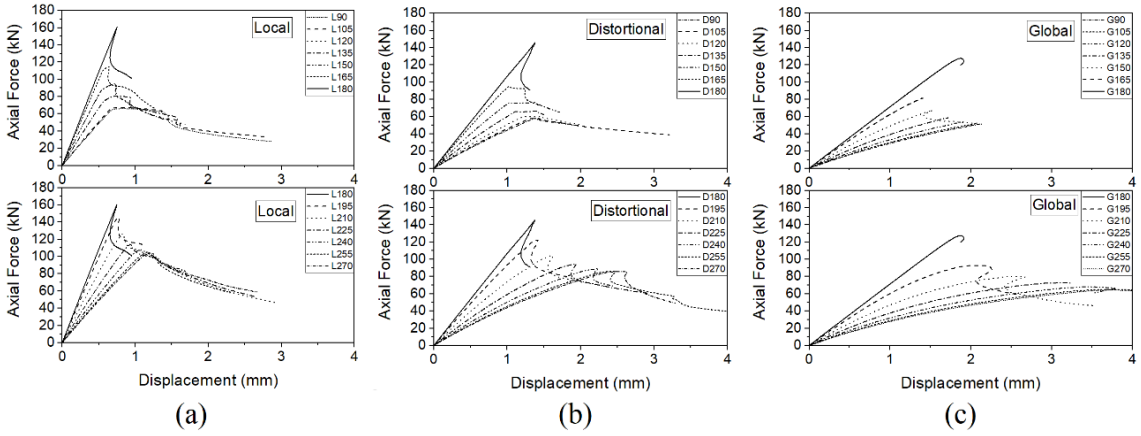

Figure 6. Axial force-displacement results for L=500 mm (a), 1000 mm (b) and 1500 mm (c).

The results in Figure 6 show that member behaviour is highly sensitive to the magnitude and the position of the eccentric load. Also, M_2^- yields higher capacity and ductility than M_1^+ because lips are in tension. Increasing axial force results in lower ductility in all specimens. And stiffness of members decreases with the increase of member length.

4 COMPARISON WITH AISI-S100-12 BEAM-COLUMN STRENGTH PREDICTIONS

For the North American Cold-Formed Steel Specification (AISI-S100-12) a simple linear interaction expression (1) for examining beam-column capacity is employed:

$$\frac{\bar{P}}{\phi_c P_n}+\frac{C_{mx}\bar{M}_x}{\phi_b M_{nx\alpha_x}}+\frac{C_{my}\bar{M}_y}{\phi_b M_{ny\alpha_y}}\le 1.0 \quad (1)$$

Nominal strength was determined for DSM in AISI-S100-12. For DSM the necessary critical elastic local and distortional buckling axial load and moments were determined using CUFSM 4.06 finite strip program assuming simply supported end boundary conditions. To automatically identify local and distortional buckling a straight-line cross-section model and a constrained finite strip method analysis performed to determine the local and distortional half-wave lengths for isolated local (L_{crl}) and distortional (L_{crd}) buckling. The second FSM analysis in CUFSM is then performed at the pre-determined L_{crl} and L_{crd} to provide the elastic buckling loads. Critical buckling lengths and load factors obtained in CUFSM is given in Table 3. Global elastic column buckling and lateral-torsional beam buckling loads were determined from CUTWP (Sarawit, 2006). Note, for global flexural buckling the full length between the reference points (150 mm is added at each end) was used, while for global torsional buckling due to warping fixity, provided by rigid beam type MPC constraint, the full specimen length was considered. For comparison purposes, a linear interaction surface constructed based on the DSM in AISI-S100-12 at the anchor points has been added to the strength interaction surface.

Table 3. Critical length and critical load factors for local and distortional buckling

P		M_1^+ (180°)		M_2^+ (90°)		M_2^- (270°)	
L_{crl} (mm)	L_{crd} (mm)	L_{crl} (mm)	L_{crd} (mm)	L_{crl} (mm)	L_{crd} (mm)	L_{crl} (mm)	L_{crd} (mm)
62.0	1179.0	62.0	634.6	42.1	1091.7	57.4	587.3
α_{crl}	α_{crd}	α_{crl}	α_{crd}	α_{crl}	α_{crd}	α_{crl}	α_{crd}
0.892	0.521	1.151	0.802	4.339	5.487	2.766	1.059

Comparisons of AISI S100-12 and the finite element results are plotted as strength surfaces in Figure 7. In each figure, all available FEM and AISI-S100-12 results are compared together by means of surface plots. To show the contribution of each limits state, the linear interaction equations for use of DSM in Sections 1.2.1 and 1.2.2 of AISI-S100-12 (Appendix-1) was implemented to provide a distinct interaction curve for yield limit, distortional limit and local limit states with the help of CUFSM, using critical load factor values. The interaction curves at particular planes in the P-M_1-M_2 space are illustrated in Figures 8-10.

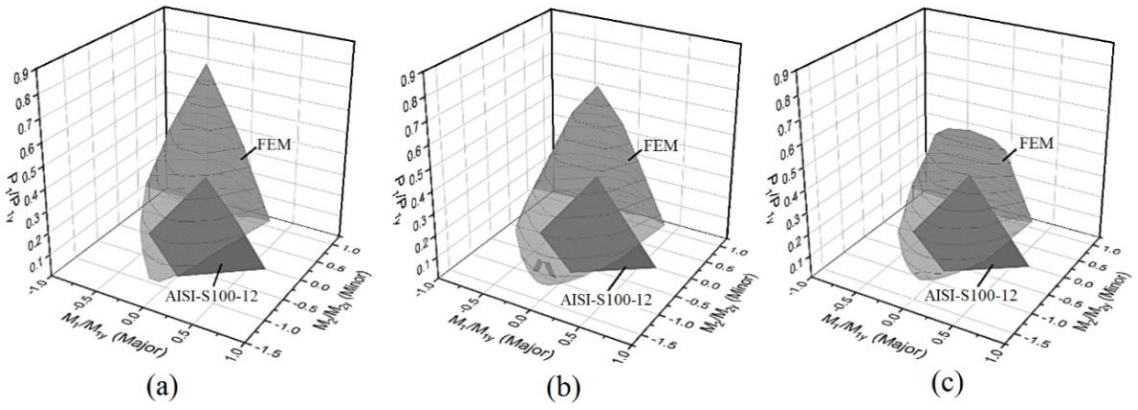

Figure 7. Comparison of FEM and AISI-S100-12 strength surfaces: L= 500 mm (a), L=1000 mm (b), L=150 mm (c)

As shown in Figures 8-10, all specimens in minor-axis bending capacities exceeding the yield strength limit state and large inelastic reserve strength is seen when lips are in tension. None of the specimens exceeded yield strength limit in major axis bending. Distortional buckling occurred in all cases prior to local buckling. This behaviour is observed in most of other sigma cross-sections given in manufacturer's catalogue. This occurs due to the intermediate stiffeners in web which prolong local buckling effect. As seen in Figures 8-10, strength difference between AISI prediction and FEM results for pure axial loading decreases with the increase of the members lengths of 500 mm, 1000 mm and 1500 mm, 34%, 26% and 1.5% respectively.

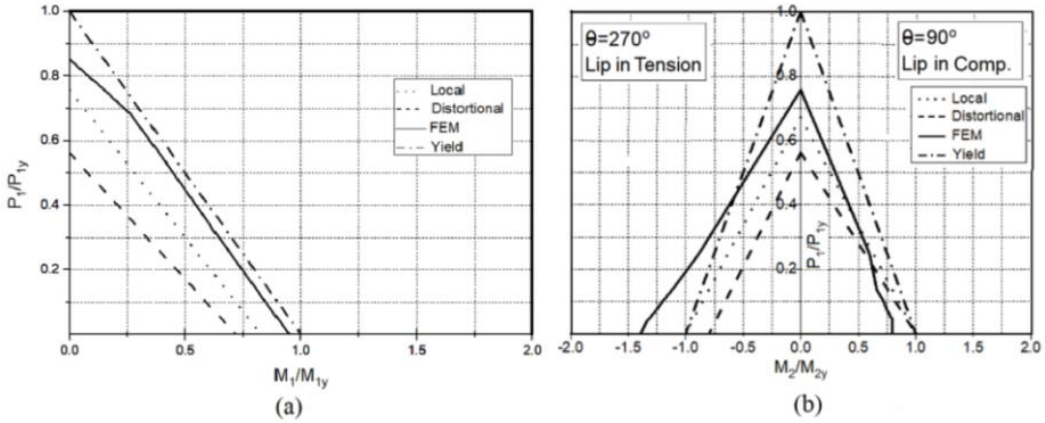

Figure 8. AISI-S100-12 and FEM results for major (a) and minor axes (b) for L=500 mm.

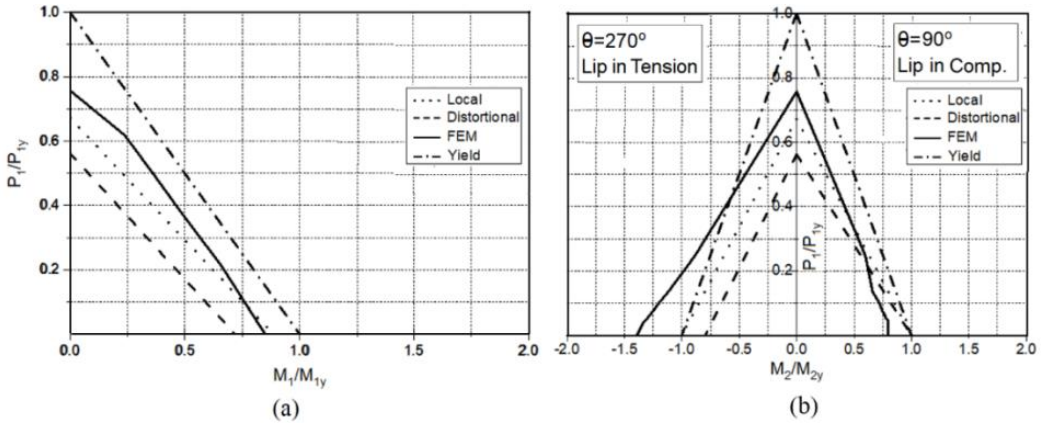

Figure 9. AISI-S100-12 and FEM results for major (a and minor axes (b) for L=1000 mm.

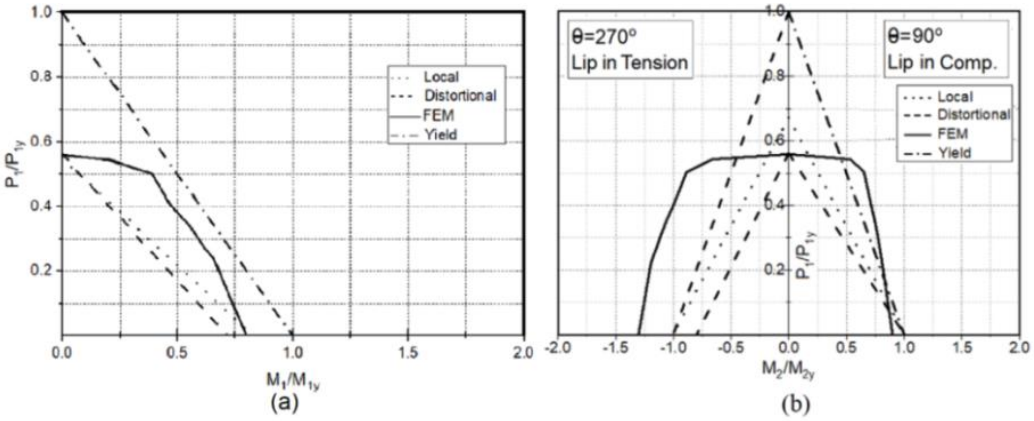

Figure 10. AISI-S100-12 and FEM results for major (a) and minor axes (b) for L=1500 mm.

5 CONCLUSIONS

A numerical program including a sigma section beam-column profiles at lengths of 500 mm, 1000 mm and 1500 mm was used to compare AISI-S100-12 specification predictions for beam-column strength with FEM results. The selected cross-section was investigated to explore beam-column performance under axial compressive load and major- and minor-axis bending on thirteen loading directions with eight loading points on each. The comparisons of FEM and AISI-S100-12 results for the beam-column members with length of 500 mm, 1000 mm and 1500 mm show that predictions using only linear interaction expressions for the beam-column strength can be excessively conservative, especially in minor axis bending when lips are in tension. it is also found that minor-axis eccentricities showed the most inelastic reserve. Increasing length results in a decrease in stiffness, and increase in axial load decreases ductility.

This study will be extended to investigate cyclic behaviour of the same sigma beam-column members to explore energy dissipation, strength and stiffness degradation behaviour.

6 REFERENCES

ABAQUS. ABAQUS/standard version 6.11. Hibbitt, Karlsson and Sorenson; 2011.

AISI-S100. (2012). North American Specification for the design of cold-formed steel structural members. Washington (DC, USA).

Amouzegar H., Amirzadeh B., Zhao X., Schafer B.W., Tootkaboni M., 2015, Statistical Analysis of the Impact of Imperfection Modes on Collapse Behavior of Cold-Formed Steel Members, Proceedings of Structural stability Research Council Annual Stability Conference, Nashville, TN, 2015.

Foroughi H., Moen C.D., Myers A.T., Tootkaboni M., Vieira L. and Schafer B.W., 2014, Analysis and Design of Thin Metallic Shell Structural Members - Current Practice and Future Research Needs, Proceedings of Structural Stability Research Council Annual Stability Conference, 2014.

Hancock, G., 2003, Cold-formed steel structures. Journal of Constructional Steel Research, 59(4), 473–487.

Li, Z., Schafer, B.W., 2010, Buckling analysis of cold-formed steel members with general boundary conditions using CUFSM: conventional and constrained finite strip methods. Proceedings of the 20th Int;l. Spec. Conf. on Cold-Formed Steel Structures, St. Louis, MO., 2010.

Macdonald, M., Heiyantuduwa, M. a., & Rhodes, J., 2008, Recent developments in the design of cold-formed steel members and structures. Thin-Walled Structures, 46(7-9), 1047–1053.,

Parastesh H, Hajirasouliha I, Taji H & Bagheri Sabbagh A, 2019. Shape Optimization of Cold-Formed Steel Beam-Columns with Practical and Manufacturing Constraints. Journal of Constructional Steel Research, 155, 249-259.

Rondal, J., 2000, Cold formed steel members and structures: General Report. Journal of Constructional Steel Research, 55, 155–158.

Sarawit, A., 2006, CUTWP Thin-walled section properties, 2006

Schafer, B. W., 2008, Review: The Direct Strength Method of cold-formed steel member design. Journal of Constructional Steel Research, 64(7-8), 766–778.

Standards Australia., 2005. Cold-formed steel structures: NZS 4600. Sydney, Australia.

Torabian, S., Zheng, B., and Schafer, B. W., 2015. Experimental response of cold-formed steel lipped channel beam-columns. Thin-Walled Structures, Elsevier, 89, 152–168.

Torabian, S., Fratamico, D. C., and Schafer, B. W.,2016b. “Experimental response of cold formed steel Zee-section beam-columns.” Thin-Walled Structures, 98, 496–517.

Ye J, Mojtabaei SM & Hajirasouliha I, 2018. Local-flexural interactive buckling of standard and optimised cold-formed steel columns. Journal of Constructional Steel Research, 144, 106-118.

Zeinoddini, V. M., & Schafer, B. W., 2012, Simulation of geometric imperfections in cold-formed steel members using spectral representation approach. Thin-Walled Structures, 60, 105–117.